Preprints, 10th IFAC International Symposium on
Advances in Automotive Control
Columbus, Ohio, USA, August 28-30, 2022

Kalman Filter-Based Integrity Monitoring for GNSS and 5G Signals of Opportunity Integrated Navigation

Mu Jia * **and Zaher M. Kassas** *

* *The Ohio State University, Columbus, OH 43210, USA*
(e-mail: jia.641@osu.edu; zkassas@ieee.org)

Abstract: A Kalman filter-based receiver autonomous integrity monitoring algorithm (RAIM) is proposed to exploit sequential measurements from global navigation satellite systems (GNSS) and cellular 5G signals of opportunity (SOPs), to ensure safe vehicular navigation in urban environments. To deal with frequent threats caused by multipath and non-line-of-sight conditions, an innovation-based outlier rejection method is introduced. Next, a fault detection technique based on solution separation test is developed, and the quantification of protection levels is derived. Experimental results of a ground vehicle traveling in an urban environment, while making pseudorange measurements to GPS satellites and cellular 5G towers, are presented to demonstrate the efficacy of the proposed method. Incorporating 5G signals from only 2 towers is shown to reduce the horizontal protection level (HPL) by 0.22 m compared to using only GPS. Moreover, the proposed method is shown to reduce the HPL and vertical protection level (VPL) by 84.42% and 69.63%, respectively, over the snapshot advanced RAIM (ARAIM).

Keywords: opportunistic navigation, Kalman filter, RAIM, solution separation, 5G.

1. INTRODUCTION

Passenger safety in automated vehicles depends on the accuracy and reliability of the vehicle's navigation system. With the continuous improvements of navigation system accuracy due to incorporation of multiple sensors (e.g., global navigation satellite systems (GNSS) receivers, lidar, camera, radar, and inertial measurement unit (IMU)), the notion of navigation integrity becomes evermore crucial as vehicles get endowed with autonomous capabilities. GNSS receivers are relied upon to calibrate sensors, correct for accumulating errors due sensor dead reckoning, and provide a navigation solution in a global frame. However, the GNSS-based navigation solution is unreliable in deep urban canyons, due to blockage, reflection, or diffraction of signals by buildings and nearby objects. Recently, cellular signals of opportunity (SOPs) have been demonstrated as a complement or alternative to GNSS signals in GNSS-challenged (Maaref and Kassas, 2020) and GNSS-denied (Kassas et al., 2022) environments. Fusing GNSS signals with cellular SOPs has shown significant improvement in the robustness, accuracy, and integrity of the navigation solution for ground (Kassas et al., 2020) and aerial (Maaref et al., 2021) vehicles.

To ensure safe navigation, automated vehicles need to tightly bound the navigation errors and ensure that the probability of navigation errors being not properly bounded is below a certain limit. Current GNSS technologies are insufficient to support the transition of ground vehicles to full automation in terms of accuracy, integrity, and availability (Zhu et al., 2020). In terms of accuracy, sub-meter-level accuracy is achievable with certain augmentation systems and real-time kinematic (RTK) only under certain favorable conditions (Humphreys et al., 2020); while single point positioning (SPP) can only achieve meter-level accuracy (Imparato et al., 2018). In terms of integrity and availability, recent work demonstrated that in a sample downtown environment (Chicago urban corridor), availability of GPS-only positioning was less than 10% at most locations. While using multi-constellation GNSS (GPS, GLONASS, Galileo, and Beidou) improved the availability significantly, it was still lower than 80% at certain locales; concluding that multi-constellation GNSS cannot provide continuous vehicle positioning (Nagai et al., 2020).

GNSS-based integrity monitoring has been extensively studied (Kropp, 2018). Among the proposed frameworks, receiver autonomous integrity monitoring algorithm (RAIM) is exceptionally attractive, as it is cost-effective and does not require installing additional infrastructure (Blanch et al., 2012). RAIM has been adapted to account for multi-constellation GNSS measurements (e.g., Galileo (Ene et al., 2006), GLONASS (Walter et al., 2013), Beidou (Liu et al., 2014), and low Earth orbit (LEO) mega-constellation-augmented GNSS (Racelis and Joerger, 2020)), aiding sensors (e.g., INS-GPS (Needham and Braasch, 2018), lidar-GNSS (Li et al., 2021), and vision-GPS (Fu et al., 2015)), and terrestrial SOPs (Maaref and Kassas, 2022). Initial studies to characterize the integrity monitoring improvement for automated driving, upon fusing GPS signals with terrestrial SOPs, were conducted in (Maaref et al., 2020; Jia et al., 2021a). However,

* This work was supported in part by the U.S. Department of Transportation (USDOT) under Grant 69A3552047138 for the CARMEN University Transportation Center (UTC) and in part by the National Science Foundation (NSF) under Grant 1929965.

these studies assumed fault-free measurements, which is not realistic in urban environments, where multipath and non-line-of-sight (NLOS) conditions are prevalent. The influence of multipath and NLOS on integrity and availability in urban environments was considered in (Jia et al., 2021b). Nevertheless, the availability rates are still not fully characterized for assured navigation.

Up until recently, most of the integrity monitoring frameworks have relied on snapshot RAIM, i.e., RAIM based on static (e.g., weighted least square) estimators, due to their straightforward projection of measurement error distribution on the solution domain. However, frequent and severe multipath effects can easily cause snapshot RAIM to fail. This is because RAIM is built on the assumption that nearly the full set of the measurements from each time-step can form a consistent set. Otherwise, snapshot RAIM is likely to fail to locate the unfaulted subset of measurements. Furthermore, multipath and NLOS errors are environment dependent, so it is difficult to model the multipath and NLOS errors as a deterministic distribution, which is a necessary prior for the threats to be monitored by RAIM. To improve the measurement redundancy, this paper develops a novel Kalman filter-based RAIM framework to fuse sequential measurements from GNSS and terrestrial SOPs. Furthermore, it introduces an innovation-based outlier rejection method to pre-filter measurement outliers. Solution separation tests are conducted to monitor and exclude faults.

This paper makes three contributions. First, a Kalman filter-based RAIM for GNSS and 5G SOP integrated navigation is proposed. Second, the technique of incorporating outlier rejection into RAIM is studied. Third, experimental results of a ground vehicle traveling in an urban environment, while making pseudorange measurements to GPS satellites and cellular 5G towers, are presented to demonstrate the efficacy of the proposed method. Incorporating 5G signals from only 2 towers is shown to reduce the horizontal protection level (HPL) by 0.22 m compared to using only GPS. Moreover, the proposed method is shown to reduce the HPL and vertical protection level (VPL) by 84.42% and 69.63%, respectively, over the snapshot advanced RAIM (ARAIM).

The paper is organized as follows. Section 2 presents the navigation system. Section 3 describes the proposed integrity monitoring framework. Section 4 presents experimental results. Section 5 concludes the paper.

2. MODEL DESCRIPTION

This section describes the GNSS and cellular pseudorange measurement models, the dynamics of the vehicle mounted receiver and cellular SOP clocks, and the extended Kalman filter (EKF)-based navigation framework.

2.1 GNSS Pseudorange Measurement Model

The ground vehicle-mounted receiver makes pseudorange measurements to M GNSS satellites from N_{const} GNSS constellations. Let $i \in \{1, \ldots, N_{\text{const}}\}$ denote the index of the constellation to which the m-th GNSS satellite belongs. The m-th GNSS pseudorange measurement at time-step k, after compensating for ionospheric and tropospheric delays, and satellite's clock bias, is modeled as

$$z_{\text{GNSS}_m}(k) = \|\boldsymbol{r}_r(k) - \boldsymbol{r}_{\text{GNSS}_m}(k)\|_2 + c \cdot \delta t_r(k) + v_{\text{GNSS}_m}(k), \quad (1)$$

where $\boldsymbol{r}_r(k)$ and $\boldsymbol{r}_{\text{GNSS}_m}(k)$ are the receiver and m-th satellite's three-dimensional (3–D) position vectors, respectively; c is the speed of light; $\delta t_r(k)$ is the receiver's clock bias; and v_{GNSS_m} is the measurement noise, which is modeled as a zero-mean white Gaussian sequence with variance $\sigma^2_{\text{GNSS}_m}(k)$.

2.2 Terrestrial SOP Pseudorange Measurement Model

The ground vehicle-mounted receiver also makes pseudorange measurements from N terrestrial SOPs, which are assumed to be stationary with known positions. The n-th SOP measurement at time-step k can be modeled as

$$z_{\text{SOP}_n}(k) = \|\boldsymbol{r}_r(k) - \boldsymbol{r}_{\text{SOP}_n}\|_2 + c \cdot [\delta t_{r,\text{SOP}}(k) - \delta t_{\text{SOP}_n}(k)] + v_{\text{SOP}_n}(k), \quad (2)$$

where $\boldsymbol{r}_{\text{SOP}_n}$ and $\delta t_{\text{SOP}_n}(k)$ are the 3–D position and clock bias of the n-th SOP transmitter, respectively; $\delta t_{r,\text{SOP}}(k)$ is the the SOP receiver's clock bias; and $v_{\text{SOP}_n}(k)$ is the measurement noise, which is modeled as a zero-mean white Gaussian sequence with variance $\sigma^2_{\text{SOP}_n}(k)$.

2.3 Receiver and Terrestrial SOP Dynamics Model

The vehicle is assumed to follow a white noise acceleration dynamics (e.g., as in (Kassas et al., 2022)). The vehicle-mounted receiver state vector is defined as $\boldsymbol{x}_v \triangleq [\boldsymbol{r}_r^\mathsf{T}, \dot{\boldsymbol{r}}_r^\mathsf{T}, \boldsymbol{x}_{\text{clk},r}^\mathsf{T}, \boldsymbol{x}_{\text{clk,SOP}}^\mathsf{T}]^\mathsf{T}$, where $\boldsymbol{x}_{\text{clk},r} = [\delta t_r, \dot{\delta} t_r]^\mathsf{T}$ is the GNSS receiver clock error state vector, with $\dot{\delta} t_r$ denoting the receiver clock drift; and $\boldsymbol{x}_{\text{clk,SOP}}$ captures the difference between the SOP receiver and each of the SOPs' transmitters clock errors.

Since the SOP pseudorange measurement (2) is parameterized by the difference between the receiver's and the SOPs' clock biases, one needs to only estimate the difference in clock biases and clock drifts. Therefore, the clock state associated with the n-th SOP can be defined

$$\Delta \boldsymbol{x}_{\text{clk,SOP}_n} \triangleq \left[c\Delta\delta t_n, c\Delta\dot{\delta} t_n\right]^\mathsf{T},$$

where $\Delta\delta t_n = \delta t_{r,\text{SOP}} - \delta t_{\text{SOP}_n}$ is the difference between the receiver's clock bias δt_r and the n-th SOP's clock bias δt_n and $\Delta\dot{\delta} t_n = \dot{\delta} t_{r,\text{SOP}} - \dot{\delta} t_{\text{SOP}_n}$ is the difference between the receiver's clock drift $\dot{\delta} t_r$ and the n-th SOP's clock drift $\dot{\delta} t_n$. The augmented clock error state is defined as

$$\boldsymbol{x}_{\text{clk,SOP}} \triangleq \left[\Delta \boldsymbol{x}_{\text{clk,SOP}_1}^\mathsf{T}, \ldots, \Delta \boldsymbol{x}_{\text{clk,SOP}_n}^\mathsf{T}\right]^\mathsf{T} \quad (3)$$

The discrete-time dynamics of $\boldsymbol{x}_{\text{clk,SOP}}$ is assumed to follow the standard double integrator model, driven by process noise (see (Bar-Shalom et al., 2002)).

2.4 EKF time and measurement update

An EKF is used to fuse the measurements from GNSS and SOPs to estimate $\boldsymbol{x}_v$. The EKF measurement update corrects the time-updated states $\hat{\boldsymbol{x}}(k+1|k)$ using available GNSS and SOP measurements. The innovation vector is computed as

$$\tilde{\boldsymbol{z}}(k+1) = \boldsymbol{z}(k) - \boldsymbol{h}\left[\hat{\boldsymbol{x}}(k+1|k)\right],$$

where $\boldsymbol{z}(k)$ the measurement vector at time-step k, and $\boldsymbol{h}(\cdot)$ is the nonlinear measurement model. The EKF

measurement-updated states $\hat{\boldsymbol{x}}(k+1|k+1)$ and associated estimation error covariance $\mathbf{P}(k+1|k+1)$ are computed using standard EKF update equations.

When a signal is fully blocked at a time-step, or detected as an outlier by prefiltering techniques, e.g., the outlier rejection method introduced in Subsection 3.2, the signal is considered as intermittent and the time-updated state estimate and prediction error covariance are passed to the next time-step, skipping the measurement update step.

3. EKF-BASED RAIM WITH OUTLIER REJECTION

This section describes the EKF-based solution separation RAIM, which fuses sequential measurements from GNSS and SOPs, to detect and exclude faults.

3.1 Framework Overview

The flowchart of the proposed EKF RAIM framework is shown in Fig. 1. The integrity monitoring system utilizes a bank of filters, among which there is one that incorporates the all in-view signals, while each of the remaining filters excludes certain signals. These two types of filters are referred to as main filter and subfilters, respectively. Each subfilter excludes one of the signals, so that the subfilter is not influenced by potential faults from the excluded signal. In order to improve the stability and availability of the system, the RAIM algorithm first screens the outliers in the measurements using the innovation-based outlier rejection method. The RAIM algorithm conducts solution separation tests to detect potential faults in the signals, and exclude detected faulty signal to maintain navigation integrity. After all the detection and exclusions, the protection level is computed based on integrity requirements.

3.2 Outlier Rejection

The outlier rejection algorithm uses the innovation filtering technique to remove measurements contaminated by severe multipath and NLOS interference caused by buildings and nearby objects. Measurements suffering from temporary biases are considered as outliers instead of faulty signals to (i) reduce the burden of fault detection and exclusion and (ii) improve measurement redundancy, as only measurement outliers for a short period of time instead of the entire duration are removed from the system. The metrics for detecting outliers is chosen to be the normalized innovation (Groves, 2013).

3.3 Solution Separation Test

This paper develops the fault detection algorithm based on the solution separation test for Kalmen filter navigation developed in (Young and McGraw, 2003; Blanch et al., 2020). The test statistics are chosen to be the difference of the position estimates from the main filter, $\hat{\boldsymbol{r}}^{(0)}(k|k)$, and the position estimates from the subfilters, $\hat{\boldsymbol{r}}^{(i)}(k|k)$. The test statistics vector can be expressed as

$$\boldsymbol{x}_{ss}^{(i)}(k) = \hat{\boldsymbol{r}}^{(0)}(k|k) - \hat{\boldsymbol{r}}^{(i)}(k|k), \qquad i = 1, \ldots, N_{ss}, \quad (4)$$

where N_{ss} is the number of subfilters, i.e., the number of faulted hypotheses to be monitored.

Young and McGraw (2003) showed that the covariance of the i-th solution separation vector can be computed as

$$\boldsymbol{\Sigma}_{ss}^{(i)}(k) = \mathbf{P}^{(i)}(k|k) - \mathbf{P}^{(0)}(k|k).$$

This enables the framework to calculate $\boldsymbol{\Sigma}_{ss}^{(i)}$ without having the cross-correlation between the main filter and subfilters.

The test threshold for the i-th hypothesis in the q-th direction is set to meet a predefined probability of false alert P_{fa} under nominal conditions,

$$T_{i,q} = Q^{-1}(\alpha_{i,q} P_{fa}) \sigma_{ss,q}^{(i)},$$

where $Q^{-1}(\cdot)$ is the inverse Q-function, $\alpha_{i,q}$ is the allocation coefficients of the false alert budget to q direction of the i-th fault mode, and $\sigma_{ss,q}^{(i)}$ is the q-th diagonal element of $\boldsymbol{\Sigma}_{ss}^{(i)}$.

3.4 Protection level computation

The protection level is a statistical error bound computed to guarantee the probability of error exceeding the bound is smaller than the defined integrity risk (Zhu et al., 2018). The predefined integrity risk budget is referred to as probability of hazardous misleading information (PHMI). Suppose that the total integrity risk budget is equally allocated to all the fault mode, the protection level in the q-th direction can be calculated by

$$PL_q = \max_i \left(T_{i,q} + Q^{-1}\left(\frac{PHMI_q}{N_{ss} P(H_i)} \right) \sigma_{ss,q}^{(i)} \right),$$

where $PHMI_q$ is the integrity budget allocated to the q-th direction, and $P(H_i)$ is the probability of the i-th fault mode. The horizontal protection level (HPL) is calculated as the the square root of the protection levels on the horizontal plane, i.e., $q = 1, 2$. The vertical protection level $VPL = PL_3$.

4. EXPERIMENTAL RESULTS

This section presents experimental results of a ground vehicle navigating with GPS and cellular 5G SOPs in an urban environment. The protection levels of the integrated GPS-SOP are compared with those of GPS only to demonstrate the performance improvement of fusing terrestrial 5G SOP measurements. The performance of the proposed framework is also compared with the snapshot ARAIM.

4.1 Experiment setup

In the experiment, a ground vehicle, mounted with antennas to receive GNSS and cellular signals, traveled on Fairview Road in Costa Mesa, California, USA. Two high-grade omnidirectional Laird antennas were connected to a quad-channel National Instruments (NI) universal software radio peripheral (USRP)-2955R to simultaneously down-mix and synchronously sample signals. The USRP were tuned to to Frequency Range 1 (FR1) 5G signals at a carrier frequency of 872 MHz and 632.55 MHz, which corresponded to the U.S. cellular provider AT&T and T-Mobile, respectively. The gNB cell IDs were 608 and 398, respectively. The 5G tower's geodetic locations were [33.652043, -117.907206, 42] and [33.670968, -117.909894, 40], which were surveyed prior to the experiment. Fig. 2 shows the environment layout.

The signals were processed in a post-processing fashion using the Multichannel Adaptive TRansceiver Information

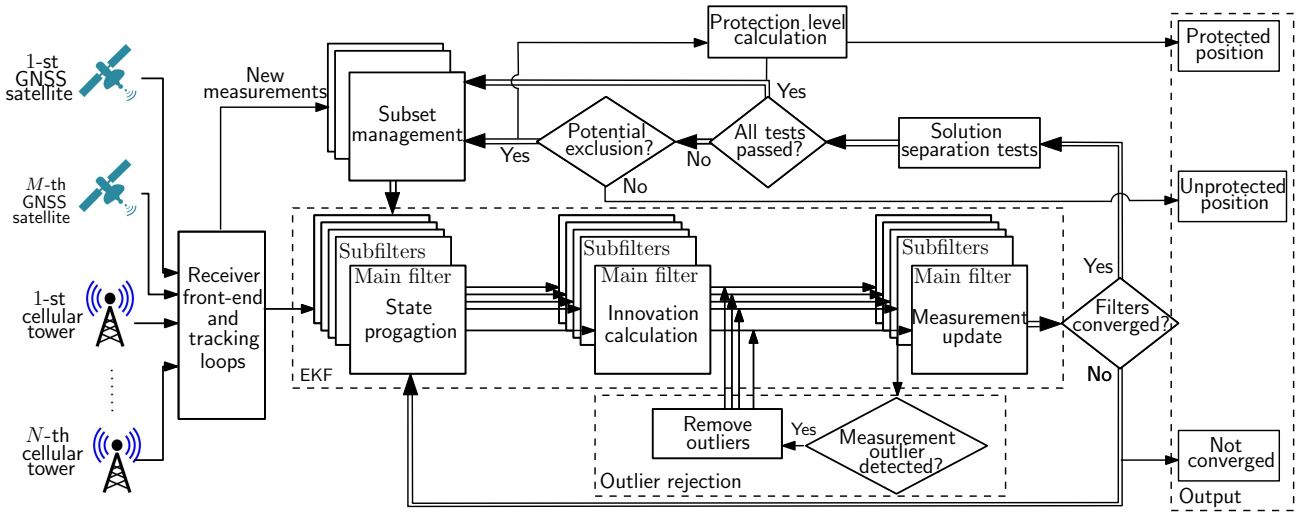

Fig. 1. Flowchart of the EKF-based RAIM with outlier rejection.

eXtractor (MATRIX) software-defined radio (SDR) (Abdallah and Kassas, 2022). The vehicle was equipped with a Septentrio AsteRx-i V integrated GNSS-IMU whose x-axis pointed toward the front of the vehicle, y-axis pointed to the right side of the vehicle, and z-axis pointed upward. AsteRx-i V is equipped with a dual-antenna multi-frequency GNSS receiver and a VectorNav VN-100 micro-electromechanical system (MEMS) IMU. The integrated GNSS receiver provides GPS pseudorange measurements, which were fed to the EKF estimator discussed in Subsection 2.4, to produce the GPS-SOP navigation solution. The tightly-coupled GNSS-IMU with satellite-based augmentation system (SBAS) navigation solution produced by AsteRx-i V was used as ground truth. The GNSS and SOP measurement rate was 5 Hz.

The budget for integrity risk were set to be 10^{-4}/h. The probability of false alert was targeted at 10^{-3}/h. The probability of fault for both GPS and 5G was set to 10^{-2}/h and the time of influence for each fault was set to 120 s. The RAIM parameters are summarized in Table 1.

Table 1. RAIM Parameters

Parameter	Definition	Value
$\{\sigma_{\text{URA,GPS}_m}\}_{m=1}^{M}$	User Range Error for GPS	5 m
$\{\sigma_{\text{URA,SOP}_n}\}_{n=1}^{N}$	User Range Error for SOP	5.48 m
$PHMI_{\text{HOR}}$	Integrity budget for the horizontal component	1.1×10^{-9}
$PHMI_{\text{VERT}}$	Integrity budget for the vertical component	1.1^{-11}
$P_{\text{fa,HOR}}$	Continuity budget allocated to the vertical component	5.6×10^{-8}
$P_{\text{fa,VERT}}$	Continuity budget allocated to the vertical component	5.6×10^{-10}
$\{P_{\text{GPS}_m}\}_{m=1}^{M}$	Probability of a single GPS satellite fault	5.6×10^{-7}
$\{P_{\text{SOP}_n}\}_{n=1}^{N}$	Probability of a single SOP fault	5.6×10^{-7}

4.2 Experimental results

During the experiment, the vehicle travelled for 125 seconds along the trajectory shown in Fig. 2. Pseudorange measurements from 9 GPS satellites and 2 5G towers were used to produce the navigation solutions. The position errors, EKF $\pm 3\sigma$ error bounds, and protection levels are plotted in Fig. 3, showing that the EKF estimator is consistent and the protection levels successfully bound the position errors.

To demonstrate the influence of fusing 5G signal on the integrity performance, the protection levels of using only GPS signals are computed and compared with the GPS+5G solution. The HPL and VPL along the trajectory for GPS+5G and GPS only are plotted in Fig. 4. The average HPL and VPL are shown in Table 2. The results show that fusing only 2 5G towers reduces the average HPL by 0.22 m at the cost of slightly increasing the VPL.

The performance of the proposed EKF-based RAIM is compared with the snapshot ARAIM using a nonlinear least-squares (NLS) estimator. Fig. 5 shows that the proposed framework significantly reduces both HPL and VPL. The average protection levels over the trajectory are given in Table 2, indicating that EKF-based RAIM reduces average HPL and VPL by 84.42% and 69.63%, respectively, over the snapshot ARAIM.

It is worth noting that using the EKF increased the root mean square error (RMSE) over NLS. This could be due to the over-simplified vehicle dynamics model adopted: white noise acceleration. The position accuracy can be improved by incorporating an IMU (Morales and Kassas, 2021; Souli et al., 2021) or using an elaborate vehicle dynamics model with well tuned parameters (Li and Jilkov, 2003).

Table 2. Performance comparison of different algorithms and signal usage

	RMSE	Avg. HPL	Avg. VPL
Snapshot RAIM with GPS only	1.1075 m	102.3792 m	53.5740 m
Snapshot RAIM with GPS+5G	1.1007 m	102.5703 m	53.7070 m
EKF RAIM with GPS only	1.1421 m	16.2013 m	16.2509 m
EKF RAIM with GPS+5G	1.1772 m	15.9801 m	16.3097 m

Fig. 2. Experiment layout and navigation solutions: ground-truth (green) and proposed framework (yellow).

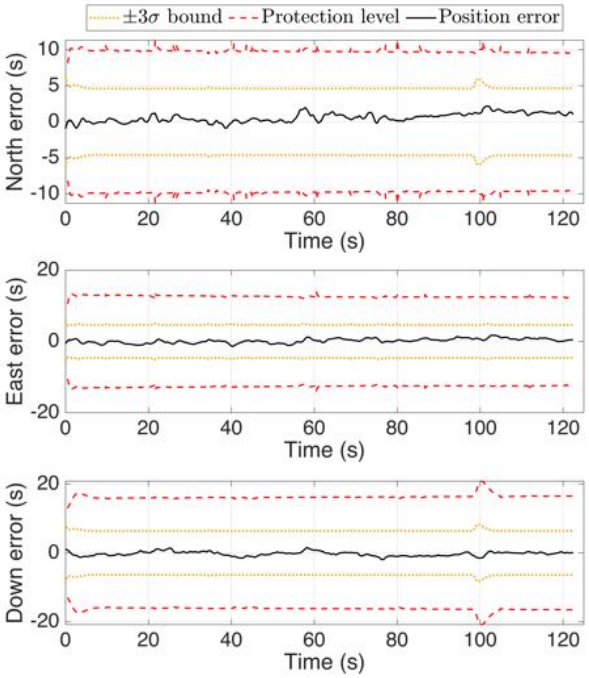

Fig. 3. EKF position errors, 3σ bounds, and protection levels with GPS and 5G signals.

5. CONCLUSION

This paper proposed a Kalman filter-based RAIM algorithm for GNSS and 5G SOP integrated navigation. To deal with frequent threats caused by multipath and NLOS conditions, an innovation-based outlier rejection method was introduced. Furthermore, a fault detection technique based on solution separation test was developed, and a quantification of protection levels was derived. The experimental results on a ground vehicle traveling in an urban environment demonstrated the efficacy of the proposed method. Incorporating cellular 5G SOPs from only 2 tower was shown to reduce the HPL by 0.22 m over using only GPS. The proposed method was also shown to reduce HPL and VPL by 84.42% and 69.63%, respectively, over the snapshot ARAIM.

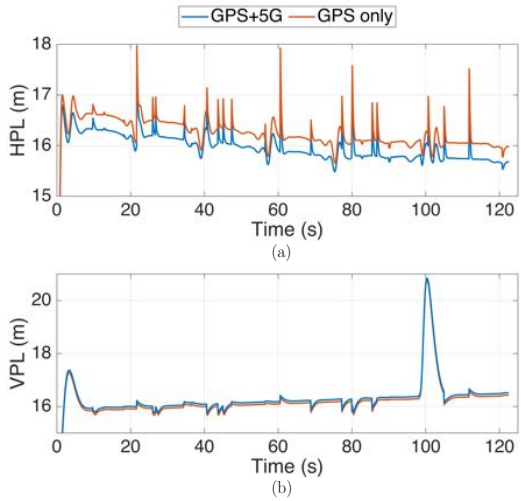

Fig. 4. Protection levels for GPS+5G and GPS only: (a) HPL and (b) VPL.

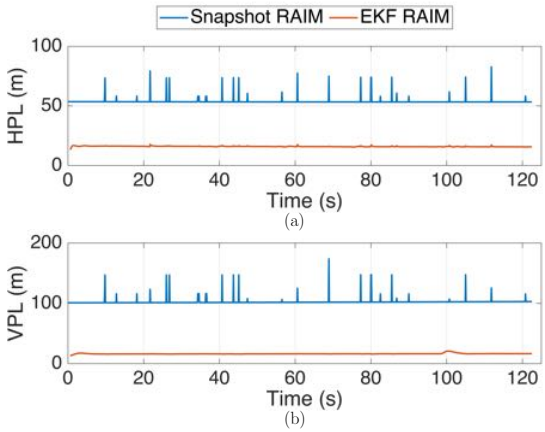

Fig. 5. Protection levels of snapshot ARAIM and EKF RAIM with GPS+5G: (a) HPL and (b) VPL.

REFERENCES

Abdallah, A. and Kassas, Z. (2022). Opportunistic navigation using sub-6 GHz 5G downlink signals: A case study on a ground vehicle. In *Proceedings of European Conference on Antennas and Propagation*, 1–5.

Bar-Shalom, Y., Li, X., and Kirubarajan, T. (2002). *Estimation with Applications to Tracking and Navigation*. John Wiley & Sons, New York, NY.

Blanch, J., Walter, T., Enge, P., Lee, Y., Pervan, B., Rippl, M., and Spletter, A. (2012). Advanced RAIM user algorithm description: Integrity support message processing, fault detection, exclusion, and protection level calculation. In *Proceedings of ION GNSS Conference*, 2828–2849.

Blanch, J., Walter, T., Norman, L., Gunning, K., and de Groot, L. (2020). Solution separation-based fd to mitigate the effects of local threats on ppp integrity. In *Proceedings of IEEE/ION Position, Location and Navigation Symposium*, 1085–1092.

Ene, A., Blanch, J., and Walter, T. (2006). Galileo-GPS RAIM for vertical guidance. In *Proceedings of National Technical Meeting of The Institute of Navigation*, 18–20.

Fu, L., Zhang, J., Li, R., Cao, X., and Wang, J. (2015). Vision-aided RAIM: A new method for GPS integrity monitoring in approach and landing phase. *Sensors*, 15(9), 22854–22873.

Groves, P. (2013). *Principles of* GNSS*, Inertial, and Multisensor Integrated Navigation Systems*. Artech House, second edition.

Humphreys, T., Murrian, M., and Narula, L. (2020). Deep-urban unaided precise global navigation satellite system vehicle positioning. *IEEE Intelligent Transportation Systems Magazine*, 12(3), 109–122.

Imparato, D., El-Mowafy, A., and Rizos, C. (2018). Integrity monitoring: From airborne to land applications. In *Multifunctional Operation and Application of GPS*, 23–43. IntechOpen.

Jia, M., Khalife, J., and Kassas, Z. (2021a). Evaluation of ground vehicle protection level reduction due to fusing GPS with faulty terrestrial signals of opportunity. In *Proceedings of ION International Technical Meeting*, 354–365.

Jia, M., Lee, H., Khalife, J., Kassas, Z., and Seo, J. (2021b). Ground vehicle navigation integrity monitoring for multi-constellation GNSS fused with cellular signals of opportunity. In *Proceedings of IEEE International Conference on Intelligent Transportation Systems*, 3978–3983.

Kassas, Z., Khalife, J., Abdallah, A., and Lee, C. (2022). I am not afraid of the GPS jammer: resilient navigation via signals of opportunity in GPS-denied environments. *IEEE Aerospace and Electronic Systems Magazine*, 37(7), 4–19.

Kassas, Z., Maaref, M., Morales, J., Khalife, J., and Shamaei, K. (2020). Robust vehicular localization and map matching in urban environments through IMU, GNSS, and cellular signals. *IEEE Intelligent Transportation Systems Magazine*, 12(3), 36–52.

Kropp, V. (2018). *Advanced receiver autonomous integrity monitoring for aircraft guidance using GNSS*. Ph.D. thesis, University of Munich, Germany.

Li, T., Pei, L., Xiang, Y., Wu, Q., Xia, S., Tao, L., Guan, X., and Yu, W. (2021). P3-LOAM: PPP/LiDAR loosely coupled SLAM with accurate covariance estimation and robust RAIM in urban canyon environment. *IEEE Sensors Journal*, 21(5), 6660–6671.

Li, X. and Jilkov, V. (2003). Survey of maneuvering target tracking. Part I: Dynamic models. *IEEE Transactions on Aerospace and Electronic Systems*, 39(4), 1333–1364.

Liu, Y., Zhang, J., Xue, R., and Wang, Z. (2014). Performance analysis of advanced RAIM with the inclusion of BeiDou. In *Proceedings of ION International Technical Meeting*, 3629–3636.

Maaref, M. and Kassas, Z. (2020). Measurement characterization and autonomous outlier detection and exclusion for ground vehicle navigation with cellular signals. *IEEE Transactions on Intelligent Vehicles*, 5(4), 670–683.

Maaref, M. and Kassas, Z. (2022). Autonomous integrity monitoring for vehicular navigation with cellular signals of opportunity and an IMU. *IEEE Transactions on Intelligent Transportation Systems*, 23(6), 5586–5601.

Maaref, M., Khalife, J., and Kassas, Z. (2020). Enhanced safety of autonomous driving by incorporating terrestrial signals of opportunity. In *Proceedings of IEEE International Conference on Acoustics, Speech and Signal Processing*, 9185–9189.

Maaref, M., Khalife, J., and Kassas, Z. (2021). Aerial vehicle protection level reduction by fusing GNSS and terrestrial signals of opportunity. *IEEE Transactions on Intelligent Transportation Systems*, 22(9), 5976–5993.

Morales, J. and Kassas, Z. (2021). Tightly-coupled inertial navigation system with signals of opportunity aiding. *IEEE Transactions on Aerospace and Electronic Systems*, 57(3), 1930–1948.

Nagai, K., Fasoro, T., Spenko, M., Henderson, R., and Pervan, B. (2020). Evaluating GNSS navigation availability in 3-D mapped urban environments. In *Proceedings of IEEE/ION Position, Location and Navigation Symposium*, 639–646.

Needham, T. and Braasch, M. (2018). Gravity model error considerations for high-integrity GNSS-aided INS operations. In *Proceedings of IEEE/ION Position, Location and Navigation Symposium*, 822–832.

Racelis, D. and Joerger, M. (2020). Impact of cascading faults on mega-constellation-augmented GNSS PPP integrity. In *Proceedings of ION GNSS Conference*, 3055–3070.

Souli, N., Makrigiorgis, R., Kolios, P., and Ellinas, G. (2021). Real-time relative positioning system implementation employing signals of opportunity, inertial, and optical flow modalities. In *Proceedings of International Conference on Unmanned Aircraft Systems*, 229–236.

Walter, T., Blanch, J., Choi, M.J., Reid, T., and Enge, P. (2013). Incorporating GLONASS into aviation RAIM receivers. In *Proceedings of International Technical Meeting of the Institute of Navigation*, 239–249.

Young, R. and McGraw, G. (2003). Fault detection and exclusion using normalized solution separation and residual monitoring methods. *NAVIGATION, Journal of the Institute of Navigation*, 50(3), 151–169.

Zhu, N., Betaille, D., Marais, J., and Berbineau, M. (2020). GNSS integrity monitoring schemes for terrestrial applications in harsh signal environments. *IEEE Intelligent Transportation Systems Magazine*, 12(3), 81–91.

Zhu, N., Marais, J., Betaille, D., and Berbineau, M. (2018). GNSS position integrity in urban environments: A review of literature. *IEEE Transactions on Intelligent Transportation Systems*, 19(9), 2762–2778.